

A catalogue of soft X-ray sources in the galactic center region

L. Sidoli¹, T. Belloni², S. Mereghetti³

¹ Astrophysics Division, Space Science Department of ESA, ESTEC, Postbus 299, NL-2200 AG Noordwijk, The Netherlands

² Osservatorio Astronomico di Brera, Via Bianchi 46, I-23807 Merate (Lc), Italy

³ Istituto di Fisica Cosmica “G. Occhialini”, CNR, via Bassini 15, I-20133 Milano, Italy

Received 12 October 2000; Accepted 4 January 2001

Abstract. We present a catalogue of 107 point-like X-ray sources derived from a systematic analysis of all the ROSAT PSPC observations of the galactic center region performed in 1992–1993. Besides SgrA*, the massive black hole at the galactic center, 41 X-ray sources have been positionally associated with already classified objects. Twenty are identified with foreground stars and five with known Low Mass X-ray Binaries. The majority of the sources in our catalogue still remains unidentified. They are hard and/or severely absorbed and probably represent a large population of X-ray binaries located in the galactic center region, accreting at low accretion rates, and still largely unknown.

Key words. Catalogues – Galaxy: center – X-rays: general – X-rays: stars

1. Introduction

The galactic center (hereafter GC) region has always been among the privileged targets of many X-ray missions. The observations made over the years established that a severe crowding of X-ray sources exists towards this part of our Galaxy (see Sidoli et al. (1999) for the results of a BeppoSAX survey of the GC with its Narrow Field Instruments). Many of the brightest sources are probably Low Mass X-ray Binaries (LMXBs) containing neutron stars or black holes, both with persistent and transient behavior, while the nature of the faintest sources is unknown. Many transient sources have been discovered in the last few years, especially during the monitoring of the galactic center region with the BeppoSAX Wide Field Camera (Ubertini et al. 1999) and the Rossi-XTE All Sky Monitor (Bradt et al. 2000).

The ROSAT Position Sensitive Proportional Counter (PSPC) performed a raster scan of the GC region ($|l| < 1.5^\circ \times (|b| < 2^\circ)$ in 1992 and 1993. The region covered is rectangular ($3^\circ \times 4^\circ$) with the major axis oriented perpendicular to the galactic plane.

We performed a detailed spatial analysis of these data with the main objective of obtaining a catalogue of X-ray sources in the soft X-ray energy band. All the data analyzed here have been retrieved from the ROSAT public archive in MPE. These datasets have previously been analyzed by Predehl & Trümper (1994) and by Predehl et

al. (1995), but neither of these works was aimed at the production of a full catalogue of sources in the region.

2. Observations and Data Reduction

The PSPC on board the ROSAT satellite (Pfeffermann et al. 1986) covered the energy band 0.1–2.4 keV with a moderate energy resolution (3–4 energy bands can be defined) and an angular resolution of $\sim 20''$ (FWHM). The detector has a circular field of view of $\sim 2^\circ$ diameter. The radial and circular supports of the entrance window produce some artifacts, whose effects are mitigated by wobbling the satellite during pointing observations.

The data consist of 43 pointed observations with exposure times in the range 2000–3000 seconds, aimed at completely covering the central part of our Galaxy with the inner region of the PSPC detector. These observations were performed between 1992 February and 1993 March. We also included in our sample a single deeper pointing (47,000 sec) centered on the Sgr A* position performed on 1992 March 2. The log of the observations is reported in Table 1.

The data have been analysed using EXSAS (Extended Scientific Analysis System, version 98APR; Zimmermann et al. 1993) implemented in the ESO-MIDAS version 97NOVpl2.0 on Sun/Solaris.

All the analysis described below was performed in four different energy ranges: 0.1–2.4 keV (channels 8–240, total energy band, T), 0.1–0.4 keV (channels 8–40, soft energy

Table 1. The PSPC observations log.

Observation ID	Pointing Direction R.A. & Dec. (J2000)	Obs. Start dd/mm/yy hh:mm	Obs. End dd/mm/yy hh:mm
rp400150n00	17 49 16.80 -30 12 00.0	04/03/92 03:48	04/03/92 04:28
rp400179n00	17 47 57.60 -30 01 48.0	02/03/92 19:53	02/03/92 20:41
rp400180n00	17 46 38.40 -29 51 00.0	02/03/92 08:49	02/03/92 09:25
rp400181n00	17 45 19.20 -29 40 48.0	02/03/92 01:11	02/03/92 03:03
rp400182n00	17 44 00.00 -29 30 36.0	01/03/92 20:06	01/03/92 20:45
rp400183a01	17 42 43.20 -29 19 48.0	28/03/93 19:56	28/03/93 20:38
rp400183n00	17 42 43.20 -29 19 48.0	02/03/92 11:54	02/03/92 12:25
rp400184n00	17 41 24.00 -29 09 00.0	01/03/92 10:26	10/03/92 12:14
rp400185n00	17 40 07.20 -28 58 48.0	29/02/92 21:38	29/02/92 22:26
rp400186n00	17 38 50.40 -28 48 00.0	29/02/92 15:16	29/02/92 19:09
rp400187n00	17 50 04.80 -29 54 36.0	03/03/92 16:37	03/03/92 10:45
rp400188n00	17 48 43.20 -29 44 24.0	03/03/92 11:52	03/03/92 17:08
rp400189n00	17 47 26.40 -29 34 12.0	02/03/92 21:33	02/03/92 22:16
rp400190n00	17 46 07.20 -29 24 00.0	03/03/92 08:40	03/03/92 09:20
rp400191n00	17 43 31.20 -29 03 00.0	04/03/92 19:49	04/03/92 20:30
rp400192n00	17 42 12.00 -28 52 12.0	01/03/92 12:00	01/03/92 17:19
rp400193n00	17 40 55.20 -28 42 00.0	01/03/92 03:56	01/03/92 04:42
rp400194n00	17 39 38.40 -28 31 12.0	29/02/92 20:04	29/02/92 20:51
rp400195n00	17 50 50.40 -29 37 48.0	03/03/92 19:50	03/03/92 20:36
rp400196n00	17 49 31.20 -29 27 00.0	04/03/92 07:01	04/03/92 07:40
rp400197n00	17 48 12.00 -29 16 48.0	03/03/92 18:13	04/03/92 13:50
rp400198n00	17 43 00.00 -28 35 24.0	02/03/92 10:20	03/03/92 15:32
rp400199n00	17 41 43.20 -28 24 36.0	01/03/92 07:13	01/03/92 07:54
rp400200n00	17 40 26.40 -28 14 24.0	29/02/92 23:15	01/03/92 00:02
rp400201n00	17 51 38.40 -29 20 24.0	03/03/92 23:07	03/03/92 23:46
rp400202n00	17 50 19.20 -29 10 12.0	04/03/92 08:37	04/03/92 09:15
rp400203n00	17 49 00.00 -29 00 00.0	04/03/92 18:09	10/03/92 15:04
rp400204n00	17 47 40.80 -28 49 48.0	04/03/92 11:56	07/03/92 10:28
rp400205n00	17 46 24.00 -28 39 00.0	02/03/92 18:18	03/03/92 13:54
rp400206n00	17 43 48.00 -28 18 00.0	01/03/92 18:21	02/03/92 15:36
rp400207n00	17 45 55.20 -28 11 24.0	01/03/92 13:42	02/03/92 13:59
rp400208n00	17 41 14.40 -27 57 00.0	01/03/92 04:51	01/03/92 06:18
rp400209n00	17 52 24.00 -29 03 00.0	04/03/92 05:23	04/03/92 06:03
rp400210n00	17 51 04.80 -28 52 48.0	04/03/92 02:13	04/03/92 02:53
rp400211a01	17 49 48.00 -28 42 36.0	23/03/93 09:24	23/03/93 09:47
rp400211n00	17 49 48.00 -28 42 36.0	03/03/92 21:56	03/03/92 22:11
rp400212n00	17 48 28.80 -28 32 24.0	16/03/93 21:06	16/03/93 21:53
rp400213n00	17 47 12.00 -28 22 12.0	16/03/93 22:42	16/03/93 23:30
rp400214n00	17 45 55.20 -28 11 24.0	02/03/92 07:06	02/03/92 07:49
rp400215n00	17 44 36.00 -28 01 12.0	01/03/92 21:34	01/03/92 22:21
rp400216n00	17 43 19.20 -27 51 00.0	01/03/92 23:10	01/03/92 23:57
rp400217n00	17 42 02.40 -27 40 12.0	01/03/92 08:48	01/03/92 09:30
rp900162n00	17 45 40.80 -29 00 00.0	02/03/92 03:56	09/03/92 05:40

band, S), 0.5–0.9 keV (channels 52–90, medium energy band, M) and 0.9–2.4 keV (91–240, hard energy band, H).

2.1. Source Detection

We first merged all the observations to produce mosaic images (with a binsize of $15''$) in the four energy bands, using only the inner part of the PSPC detector. In fact the pointing directions were appropriately defined to continuously map the region with the inner part of the detector, that provides the best sensitivity and angular resolution (adding the overlapping outer regions with a different

Point Spread Function would degrade the image quality). The corresponding exposure images were also produced in the four energy bands.

The final mosaic in the total energy band, corrected both for the different exposure times and for the vignetting, is displayed in Fig. 1. The corresponding (vignetted) exposure map, used to correct it, is shown in Fig. 2.

We then applied, for each energy band, a source detection algorithm based on the following steps:

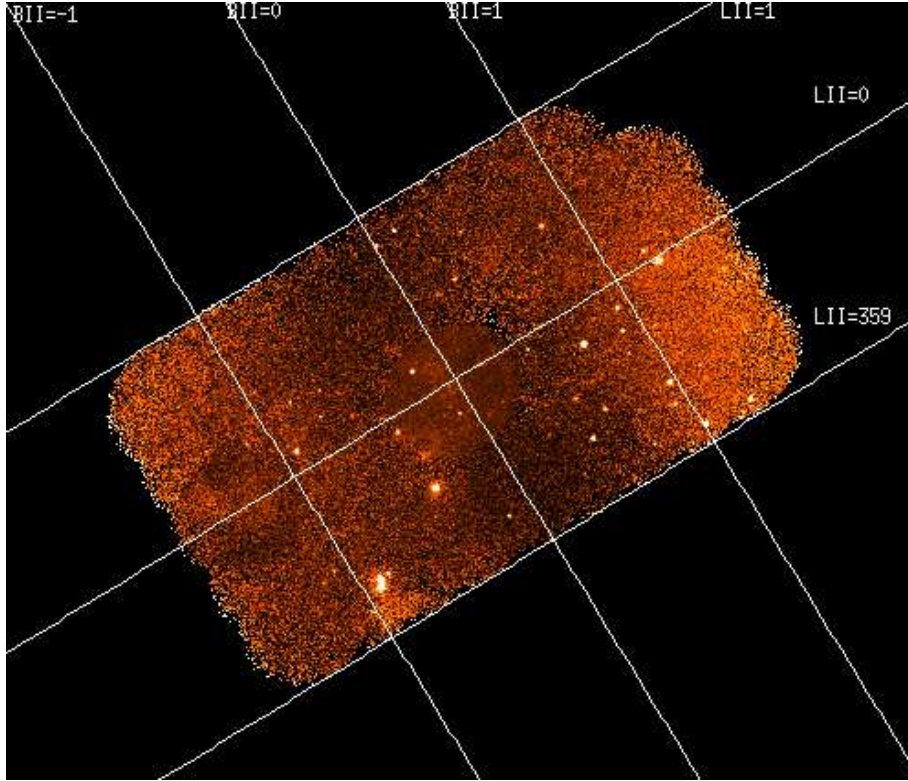


Fig. 1. Mosaic image of the galactic center region in the 0.1-2.4 keV energy range. Only the inner part of the PSPC detector has been used. The image has been corrected for the exposure and for the vignetting

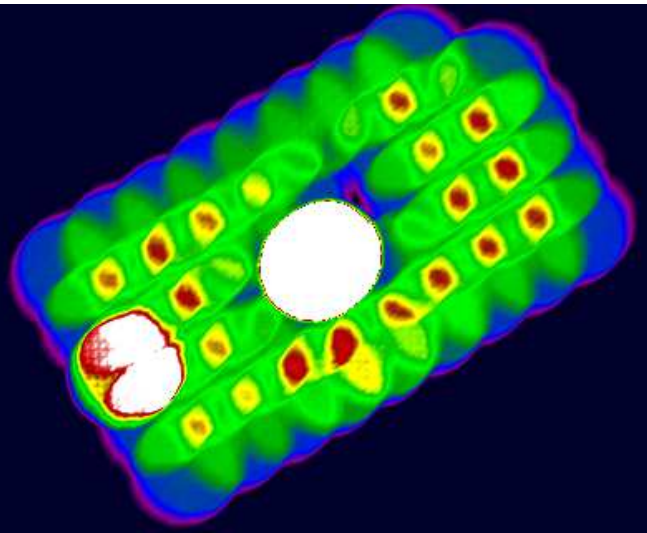


Fig. 2. Exposure map appropriate for the PSPC mosaic in the total energy band

– *local-detection algorithm*: consisting of a sliding window technique, where a detection cell of 3×3 pixels is

shifted across the images. The total counts inside the detection cell are compared with a local background taken from the 16 pixels surrounding the detection cell itself. A 3σ detection threshold has been applied. This local detection is used to produce a preliminary list of sources.

- *production of a smoothed background image*: the source list produced in the previous step is used to remove from the image circular regions around each source position. The resulting source-free image is fitted by a two-dimensional spline function to fill the holes and to produce a background image. A background image is produced for each energy band.
- *map-detection algorithm*: a new sliding window search is performed, this time using the background image to extract information about the local background. In other words, for each detection cell, the corresponding background is extracted, not from a frame surrounding it, but from the background map at that position. A second list of sources is produced, again with a 3σ detection threshold.
- *merging of the source lists*: the two lists of sources resulting from the two sliding window searches are merged together, removing duplicates in order to have a unique list of sources (in each energy band).

Duplicates are removed checking whether the distance between two sources is less than twice the sum of the size of the detection windows or less than the FWHM of the point spread function of the instrument.

- *maximum-likelihood method*: a maximum-likelihood method (Cruddace et al. 1987) is then applied to the photon lists, using the merged list of sources as candidates. This method considers the ROSAT PSPC point spread function and the position of the source inside the detector and derives a source position and an existence likelihood. Only a detection likelihood larger than 10 (corresponding to a probability of a chance detection smaller than e^{-10}) was considered as a true source. A final list of sources with their positions and positional uncertainties is thus produced.

This process yielded four lists of sources (one for each energy band).

The same procedure was also applied on the individual observations, this time also considering the external part of the PSPC detector, resulting in 4×43 lists of sources (4 energy bands and 43 observations). This second search was motivated by the fact that, e.g. due to source variability, some sources might have been missed in the previous global analysis.

Finally, all the lists of detected sources were cross correlated in order to clean the catalogue, removing all the sources with a multiple detection. By multiple detection we mean two or more sources whose position is compatible with each other, in which case only the source with higher existence likelihood has been kept. This procedure yielded a final catalogue containing 107 sources.

The count rates and upper limits (2σ) in each energy band have been extracted from the photon events tables at the position of the detected sources. Two softness ratios have been also derived: S/H and M/H, where H, M and S are the net source counts in the hard, medium and soft energy bands defined in Sect. 2.

3. The catalogue of galactic center sources

The spatial distribution of the sources detected in the surveyed region is displayed in Fig. 3. The remarkable symmetry of this distribution, and in particular the rather uniform source density as a function of galactic latitude, probably indicates that many sources are at a distance much closer than that of the galactic center. The final catalogue is reported in Table 3, where for each source the identification number, coordinates (J2000), count rate in the total energy band (0.1–2.4 keV), softness ratios S/H and M/H and possible identifications are reported. It is possible that a source has an upper limit in the total energy band, but is detected in one of the single energy bands. This is due to the energy-dependent background: faint sources detected, for example, in the hard energy range, could have been missed in the total energy band due to a higher background level. For these sources, the count rate in the energy band where a detection has been

found is shown (and marked). On the other side, a few sources have been detected in the total energy band, but have only upper limits in all the other energy ranges; in this case the softness ratios are missing from Table 3. In Figs. 4 and 5 the two softness ratios versus the count rate in the total energy band are shown.

A ROSAT PSPC count rate of 0.01 counts s^{-1} corresponds to about 5×10^{-11} ergs cm^{-2} s^{-1} (unabsorbed flux), assuming a 5 keV bremsstrahlung spectrum and a column density of 6×10^{22} cm^{-2} .

4. Discussion

The application of the maximum-likelihood method to 43 pointings of the GC region performed with the ROSAT PSPC instrument in 1992–1993 has led to a new catalogue of soft X-ray sources. Our catalogue contains 107 detections, down to a count rate of ~ 0.001 counts s^{-1} in the energy range 0.1–2.4 keV.

A correlation with the SIMBAD database resulted in probable identifications based on positional coincidence. The most plausible identifications (objects falling inside the PSPC error circle) are reported in Table 3. Other candidate counterparts (IRAS sources, for example) whose positions fall outside the PSPC error are also listed, when their large error boxes overlap with the ROSAT error box. For the possible counterparts listed in column (8) we give in parenthesis the distance between the optical and X-ray positions, the spectral type and magnitudes for stars, and other relevant informations as described in the notes to Table 3.

4.1. X-ray binaries

Our discovery of ROSAT counterparts to a few previously known X-ray sources, allows us to significantly improve their positions. This is the case of the recently discovered 729 sec X-ray pulsar AXJ 1740.2–2848 (Sakano & Koyama 2000, later named AX J1740.1–2847 by Sakano et al. 2000) and of the other two ASCA sources AX J1744.3–2940 (Sakano et al. 1999a) and AX J1740.3–2904 (Sakano et al. 1999b).

We also inspected the error boxes of the X-ray binaries indicated in Table 2, without finding any ROSAT counterparts in our catalogue, within a radius of $1'$ of their position.

4.2. Foreground Stars

A number of ROSAT sources have stellar counterparts in their error circles (see Table 3). To test these associations, we computed the $\log(f_X/f_{opt})$ as in Voges et al. (1999), using a constant conversion factor of 1.48×10^{-11} ergs cm^{-2} cts^{-1} , appropriate for stellar sources (Fleming et al. 1995). The derived optical to X-ray flux ratios are displayed in Fig. 6 as a function of the count rate in the total energy band.

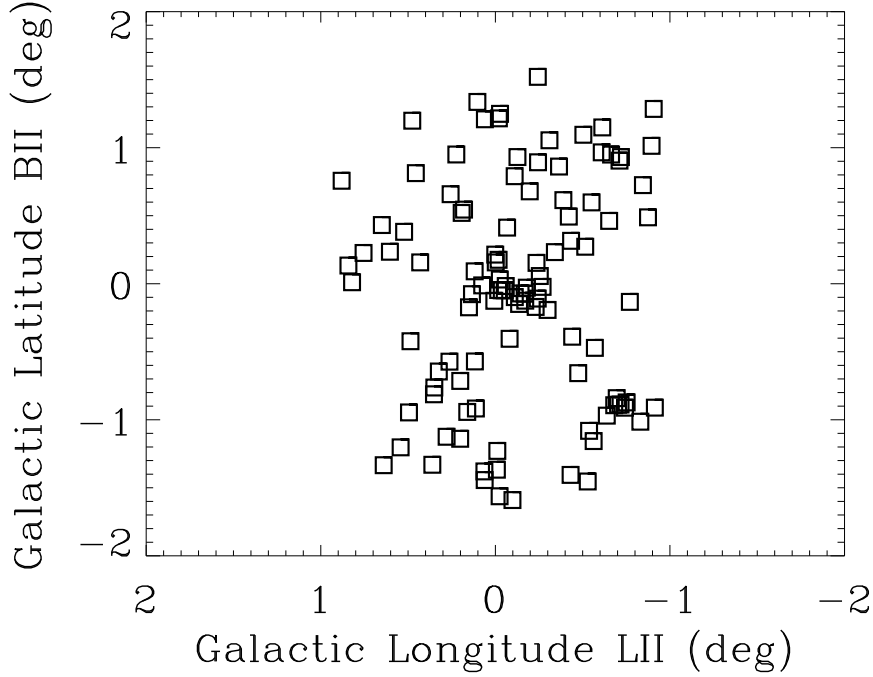


Fig. 3. Distribution of the ROSAT sources detected in the galactic center region

Table 2. X-ray sources not detected

Source	Reference
1E 1743.1–2843	Cremonesi et al. 1999
XTE J1748–288	In 't Zand et al. 1998
KS 1741–293	In 't Zand et al. 1990
GX+1.1–1.0	Proctor et al. 1978
GX+0.2–1.2	Proctor et al. 1978
GRS 1741.9–2853	Sunyaev et al. 1991
GRS 1734–29	Sunyaev et al. 1991b
GRS 1743–290	Cordier et al. 1993
GRS 1747–312	Pavlinksi et al. 1994
GRS 1747–341	Cordier et al. 1993
1E 1742.5–2845	Watson et al. 1981
1E 1742.7–2902	Watson et al. 1981
1E 1742.9–2849	Watson et al. 1981
1E 1743.1–2852	Watson et al. 1981
1E 1741.2–2859	Mitsuda et al. 1990
GC X–2	Cruddace et al. 1978
GC X–4	Cruddace et al. 1978
XTE J1755–324	Remillard et al. 1997
GRO J1744–28	Lewin et al. 1996
SAX J1750.8–2900	Bazzano et al. 1997
1E 1740.7–2942	Mirabel et al. 1992
SAX J1747.0–2853 = GX 0.2–0.2	In 't Zand et al. 1998b
XTE J1739–285	Markwardt et al. 1999
GRS 1739–278	Paul et al. 1996

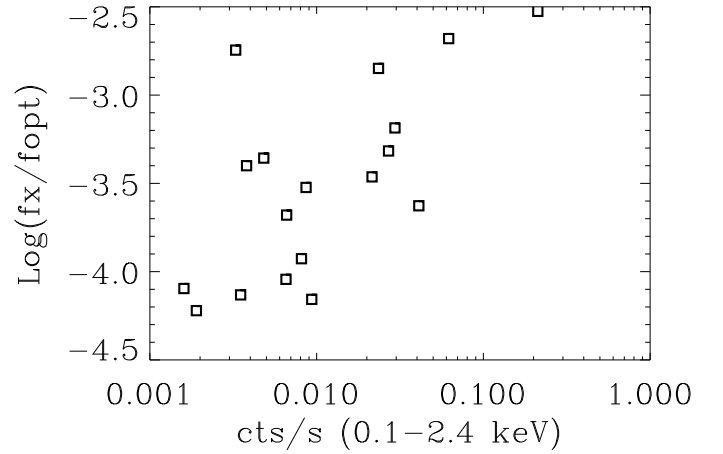


Fig. 6. $\log(f_X / f_{\text{opt}})$ as a function of the source count rate in the total energy band (0.1–2.4 keV) for the sources identified with stars

the basis of the ratio between their X-ray to optical flux, all these sources could indeed be stellar X-ray sources.

From Figs. 4 and 5 it can be seen that the sources tentatively identified with stars have relatively softer (or less absorbed) spectra.

Stars usually have $\log(f_X / f_{\text{opt}})$ values in the range $[-6, -1]$, depending on the spectral type. Therefore, on

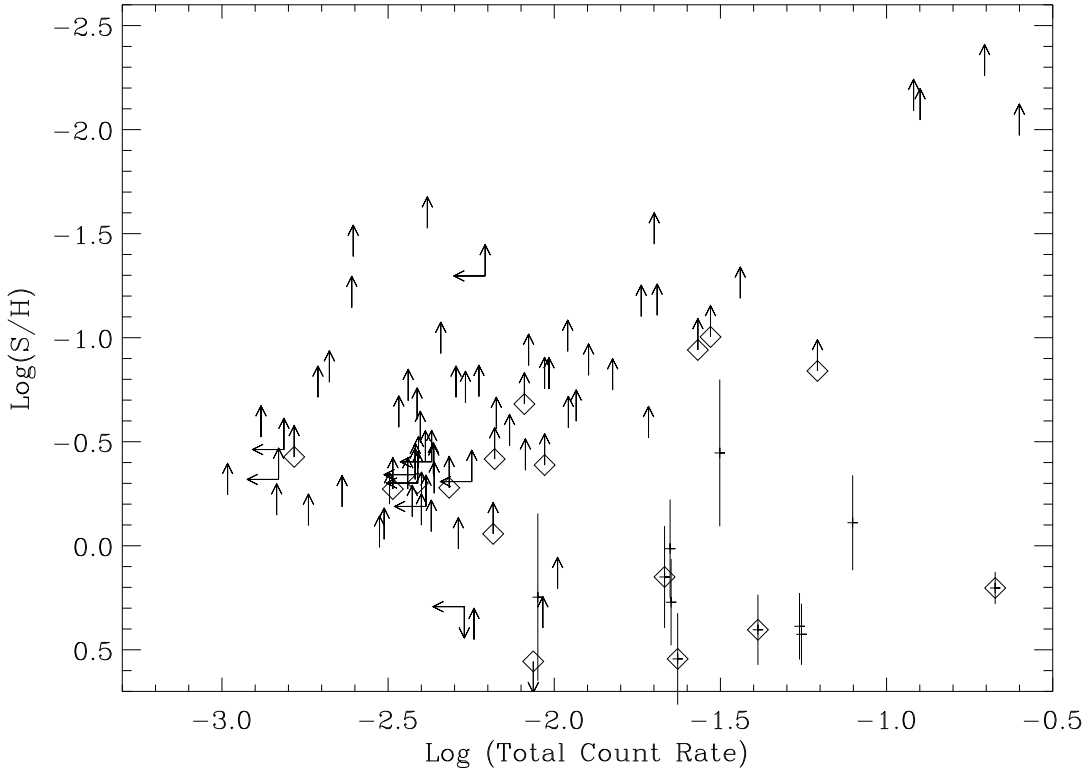


Fig. 4. Softness ratio S/H as a function of the source count rate in the total energy band (0.1–2.4 keV). The upper limits on the total count rate refer to the sources that were detected only in the Soft or in the Hard energy bands. All the error bars are at 1σ and the upper/lower limits at 2σ . The square symbols mark the sources possibly identified with stars

4.3. Supernova Remnants

We searched for the possible association of ROSAT sources with galactic supernova remnants.

The inspection of the Green catalogue of all the SNRs (Green 1998) located in the region shows that no ROSAT point sources in our catalogue fall inside the region covered by the following supernova remnants: G0.3+0.0, G0.9+0.1, G1.0–0.1 and G359.1–0.5.

Two ROSAT sources (n 81 and n 71) fall on or nearby the northern part of the radio shell of G359.0–0.9 (23′ size). Source n 3 is located at the center of the shell like SNR 359.1+0.9 (11′×12′ size). This source can also be associated with the star HD316072 (see Sect. 4.2). Diffuse X-ray emission has been recently detected with ASCA from the G359.0–0.9 shell and, marginally, from 359.1+0.9 (Sakano et al. 1999).

5. Conclusions

The spatial analysis, using a maximum-likelihood method, applied to public ROSAT PSPC data of the GC region led to the detection of 107 point-like sources, down to a PSPC count rate of 0.001 counts s^{-1} in the 0.1–2.4 keV energy range.

Using the SIMBAD database, 42 sources have been associated with objects at other wavelengths; 20 are probably stars and 5 have been identified with previously known LMXBs. Other sources have been already classified as X-ray objects, but their nature is still uncertain. Two sources in our catalogue could be associated with shells of supernova remnants and one with a molecular cloud or a maser source (n 72).

An error circle of 1′ radius centered on the positions of 25 LMXBs known to lie inside the region surveyed with PSPC has been inspected, leading to negative results.

All the sources brighter than 0.060 counts s^{-1} have been positionally associated with known objects.

The majority of our sources still remains unidentified. They are mostly undetected in the soft and medium PSPC energy ranges, they are quite hard and/or severely absorbed. Their average count rate in the total energy band (0.01 counts s^{-1}) translates into a luminosity in the range 10^{35} – 10^{36} erg s^{-1} (assuming a distance of 8.5 kpc) which is suggestive of mass-transfer from a companion star onto a compact object in a binary system.

We propose that these still unidentified sources belong to a large population of X-ray binaries located in the GC region, accreting at low accretion rates, and still largely unknown. The transient sources recently discovered with

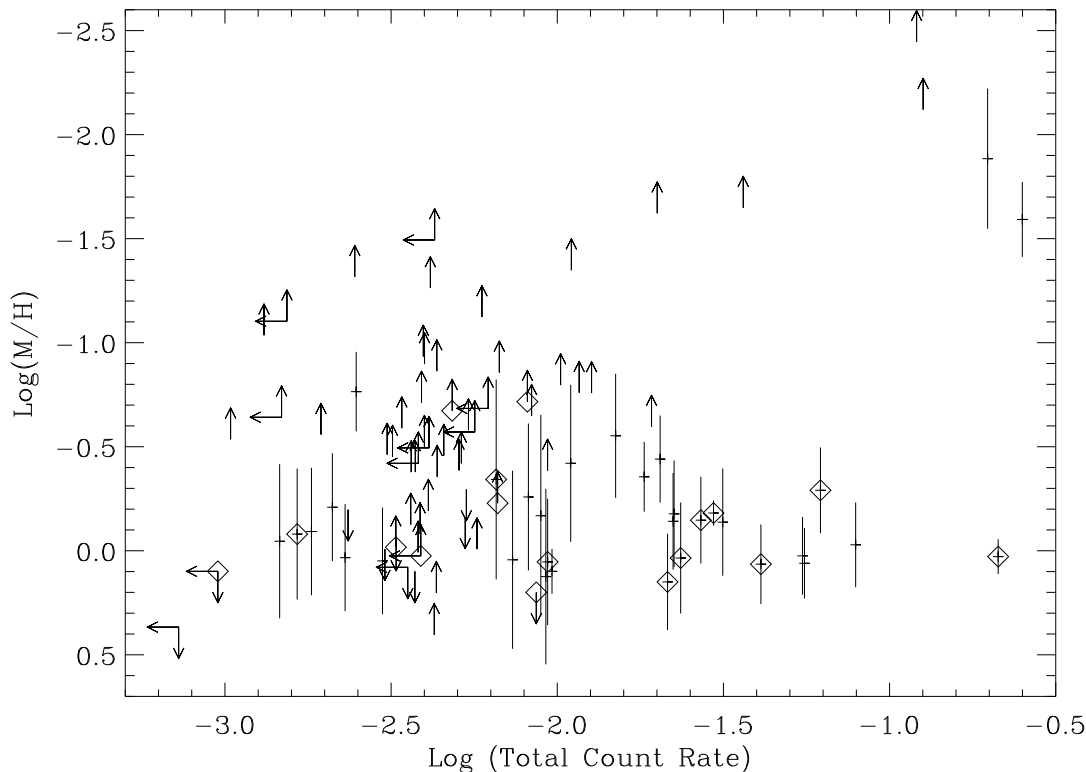


Fig. 5. Softness ratio M/H as a function of the source count rate in the total energy band (0.1-2.4 keV). The upper limits on the total count rate refer to the sources that were detected only in the Medium or in the Hard energy bands. All the error bars are at 1σ and the upper/lower limits at 2σ . The square symbols mark the sources possibly identified with stars

ASM–XTE and WFC–BeppoSAX would be only the high luminosity tail of this population of LMXBs.

Acknowledgements. We have made use of the ROSAT Data Archive of the Max Planck Institut für extraterrestrische Physik at Garching; and of the SIMBAD database operated at Centre de Données astronomiques in Strasbourg. We thank A. Parmar for reading this manuscript and providing helpful comments. L.Sidoli acknowledges an ESA Fellowship.

References

- Bazzano A., Heise J., Ubertini P., et al., 1997, IAU Circ. 6597
- Bradt H., Levine A.M., Remillard R.A., Smith D.A., 2000, In “X-ray Astronomy 1999; Stellar Endpoints, AGN and the Diffuse Background”, Bologna, Sep. 1999, Eds. G.Malaguti, G.Palumbo and N.White, pub. Gordon and Breach, in press (astr-ph/0003438)
- Cordier B., et al., 1993, In “The Second Compton Symposium”, AIP 304, Eds. C.E.Fichtel, N.Gehrels and J.P.Norris (New York), 446
- Cremonesi D.I., Mereghetti S., Sidoli L., Israel G.L., 1999, A&A 345, 826
- Cruddace R.G., Hasinger G.R., Schmitt J.H.M.M. 1987, In “Astronomy from Large Databases”, Murtaugh F., Heck A. (eds.), p.177
- Cruddace R.G., Fritz G., Shulman S., et al., 1978, ApJ 222, L95
- Green D.A., 1998, In “A catalogue of galactic Supernova Remnants”, [HTTP://WWW.MRAO.CAM.AC.UK/SURVEYS/SNRS/](http://www.mrao.cam.ac.uk/surveys/snrs/)
- Fleming T.A., Molendi S., Maccacaro T., Wolter A., 1995, ApJ Suppl.Ser. 99, 701
- In ’t Zand J.J., Heise J., Smith M., et al., 1998, IAU Circ. 6840
- In ’t Zand J.J., Bazzano A., Cocchi M., et al., 1998b, IAU Circ. 6846
- In ’t Zand, et al., 1990, Adv. Space Res. 11, 187
- Lewin W.H.G., Rutledge R.E., Kommers J.M., et al., 1996, ApJ., 462, L39
- Markwardt C.B., Marshall F.E., Swank J.H., et al., 1999, IAU Circ. 7300
- Mirabel F., Rodriguez L.F., Cordier B., et al., 1992, Nat 358, 215
- Mitsuda K., Takeshima T., Kii T., Kawai N., 1990, ApJ 353, 480
- Paul J., Bouchet L., Churazov E., Sunyaev R., 1996, IAU Circ. 6348
- Pavlinkii M., Grebenev S.A., Sunyaev R.A., 1994, ApJ 425, 110
- Pfeffermann E., Briel U.G., Hippmann H., et al. 1986, SPIE 733, 519
- Predehl P., Trümper J., 1994, A&A 290, L29
- Predehl P. et al. 1995, in “Nuclei of Normal Galaxies”, eds. R. Genzel & A.I. Harris (NATO ASI Ser. C, 445), (Dordrecht:Kluwer), 21
- Proctor R.J., Skinner G.K., Willmore A.P., 1978, MNRAS 185, 745

- Remillard R., Levine A., Swank J., Strohmayer T., 1997, IAU Circ. 6710
- Sakano M., Imanishi K., Tsujimoto M., et al., 1999a, ApJ 520, 316
- Sakano M., Yokogawa J., Mukarami H., et al., 1999b, In Proc. of the “Japanese German Workshop on High Energy Astrophysics”, eds. Becker W. & Itoh W., MPE Report 270, 113
- Sakano M., Koyama K., 2000, IAU Circ. 7364
- Sakano M., Torii K., Koyama K., et al., 2000, PASJ 52, in press (astro-ph/0008331)
- Sidoli L., Mereghetti S., Israel G.L., et al., 1999, ApJ 525, 215
- Sunyaev R.A., Pavlinskii M., Churazov E., et al., 1991, SovA. Lett. 17, 42
- Sunyaev R.A., Churazov E., Gilfanov M., et al., 1991b, Adv. Space Res. 11, 177
- Te Lintel Hekkert P., Versteeg-Hansel H.A., Habing H.J., et al., 1989, A&AS 78, 399 (TVH89)
- Ubertini P., Bazzano A., Cocchi M., et al., 1999, Proc. “Third INTEGRAL Workshop”, Taormina 1998, Astroph. Lett. and Communications 38, 301
- Voges W., Aschenbach B., Boller Th., et al., 1999, A&A 349, 389
- Watson M.G., Willingale R., Grindlay J.E., et al., 1981, ApJ 250, 142
- Zimmerman H.U., Becker W., Belloni T., et al., 1994, EXSAS User’s Guide, MPE Report 257

Table 3. The ROSAT PSPC Catalogue. The numbers in parenthesis in the first column refer to the sources detected by Predehl & Trümper (1994). In column n.5 sources not detected in the total (T) energy band, but only in a partial (S,M or H) band, are labelled with a capital letter. Column n.8 reports the probable identifications based on the cross-correlation with SIMBAD database; in parenthesis we indicate the offset, spectral type, B and V magnitude for stars. The meaning of the other symbols is: Al*=Eclipsing Binary of Algol type; V*=variable star; bL*=Eclipsing Binary of beta Lyr type; *i*= star in double system; Em*=emission line star; IR=infrared source

Source ID	R.A. (J2000)	Dec. (J2000)	Error (")	cts ks ⁻¹ (0.1–2.4 keV)	Log(S/H)	Log(M/H)	Notes
1	17 38 26.3	-29 01 47.2	6.2	79 ±6.93	-0.111 ± 0.228	-0.0287 ± 0.203	RXJ1738.4-2901
2	17 39 08.6	-28 20 32.5	14.9	11.1 ±2.27	–	–	
3	17 39 31.1	-29 09 50.3	8.9	61.9 ±5.86	< -0.840	-0.291 ± 0.206	HD316072 (3"; K0;B=11.2;V=9.97); at the center of G359.1+0.9
4	17 39 40.9	-28 51 11.3	10.0	6.61 ±1.36	< -0.416	< -0.229	V846 Oph (1"; (Al* V*) A2; B=10.32; V=9.90)
5	17 40 09.2	-28 47 23	11.4	5.06 ±1.17	< -0.713	< -0.386	AXJ 1740.2-2848 (pulsar)
6	17 40 15.9	-29 03 32.1	10.0	19.2 ±2.54	< -0.519	< -0.597	AXJ1740.3-2904
7	17 40 19.9	-29 00 4.90	9.8	4.34 ±1.30	< -0.334	< -0.863	
8	17 40 23.2	-29 03 58.2	20.9	5.73 ±1.52	< 0.451	< -0.00757	
9	17 40 24.0	-28 56 50.5	3.6	55.4 ±3.23	0.425 ± 0.147	0.0601 ± 0.169	1RXSJ174024.6-285700 (18")
10	17 40 41.2	-28 08 50.0	16.0	3.73 ±1.2	–	> 0.0988	
11	17 40 42.7	-28 18 13.4	1.4	251 ±6.75	< -1.97	-1.59 ± 0.180	RXJ1740.7-2818 (11"); 1E1737.5-2817 (47")
12	17 40 45.6	-29 16 31.3	11.9	10.2 ±2.15	< 0.2067	< -0.796	
13	17 40 46.7	-28 38 48.1	9.8	9.24 ±1.73	< 0.395	0.124 ± 0.422	
14	17 40 51.4	-28 18 56.0	14.8	4.26 ±1.32	< -0.0684	< 0.404	
15	17 41 04.4	-28 15 4.3	5.0	22.3 ±2.14	0.0140±0.236	-0.141 ± 0.232	
16	17 41 23.7	-28 47 43.0	9.1	8.92 ±1.60	0.247 ± 0.402	-0.169 ± 0.484	
17	17 41 33.8	-28 40 35.0	5.9	20.3 ±1.92	< -1.107	-0.441 ± 0.209	
18	17 41 36.7	-29 25 30.6	22.5	4.32 ±1.22	< -0.345	< 0.202	
19	17 41 41.8	-28 33 22.1	6.4	22.4 ±2.08	0.271 ± 0.208	-0.177 ± 0.256	
20	17 41 58.0	-29 05 34.5	5.0	21.5 ±1.97	0.15 ± 0.24	0.150 ± 0.231	HD160572 (2"; F3V ;B=9.59;V=9.16)
21	17 42 06.5	-27 54 12.5	18.7	3.07 ±0.9	–	–	
22	17 42 15.2	-29 14 59.2	3.2	54.70 ±3.43	0.387 ± 0.16	0.0245 ± 0.187	
23	17 42 16.9	-28 37 1.2	16.9	3.99 ±1.00	< -0.203	< -0.897	
24	17 42 17.5	-28 56 47.6	11.6	3.98 ±1.11	< -0.099	< -0.499	
25	17 42 27.8	-28 14 55.9	13.0	2.1 ±0.7 ^(H)	< -0.342	< -0.421	
26	17 42 30.3	-28 44 56.3	1.8	212 ±6.65	0.203 ± 0.077	0.0280 ± 0.0836	V2384 Oph (1"; (bL* V*) G3/G5V; B=9.75; V=9.02)
27	17 42 41.3	-29 02 13.6	8.7	11.6 ±1.45	< -0.599	< -0.760	
28	17 43 19.5	-29 14 1.10	15.7	5.40 ±1.14	< -0.688	< -0.579	
29	17 43 21.0	-29 08 29.9	19.2	3.1 ±0.99	< -0.0307	< -0.462	
30	17 43 32.7	-28 07 25.0	5.5	23.5 ±1.9	0.544 ± 0.220	0.0348 ± 0.267	HD316199 (2"; K5; B=10.6)
31	17 43 40.2	-28 22 27.7	52.0	1.9 ±0.7 ^(H)	< -0.302	< 0.0246	HD316212 (47"; K5; B=11.3; V=9.9)
32	17 43 51.1	-28 46 43.7	11.6	11.0 ±1.94	< -0.934	-0.420 ± 0.377	
33	17 43 53.8	-29 06 21.9	15.1	2.7 ±1.0 ^(H)	< -0.308	< -0.571	IRAS17407-2904 (44")
34	17 43 55.6	-28 29 57.9	14.1	4.09 ±1.23	< -0.402	< -0.192	IR [OF84] 18 (37"); IRAS 17407-2829 (49")
35	17 44 03.1	-28 30 1.5	15.3	5.33 ±1.4	–	> -0.295	
36	17 44 17.6	-29 39 48.0	6.6	14.9 ±1.79	< -0.748	-0.553 ± 0.298	AXJ1744.3-2940 (19")

Table 3. Continued

Source ID	R.A. (J2000)	Dec. (J2000)	Error (")	cts ks ⁻¹ (0.1–2.4 keV)	Log(S/H)	Log(M/H)	Notes
37	17 44 27.4	-29 03 29.7	8.4	2.9 ±0.356	< 0.00717	0.0489±0.256	
38	17 44 46.2	-27 47 27.3	17.4	5.3 ±2.0	–	> -0.161	
39	17 44 47.0	-28 49 28.3	17.3	1.27 ±0.316	–	–	
40	17 44 47.3	-29 07 27.9	13.9	2.3 ±0.355	–	> -0.198	
41	17 44 53.3	-28 51 39.3	10.0	2.8 ±0.4 ^(H)	< -0.404	< -1.494	IR MGM 1–3 (6")
42 (4)	17 45 00.1	-28 51 24.9	15.0	3.9 ±0.436	< -0.495	< -0.934	1E 1741.7–2850 (56")
43	17 45 03.8	-29 10 47.8	16.2	1.2 ±0.279	–	–	IR GCS13 (18")
44 (13)	17 45 18.1	-29 06 21.4	10.5	1.3 ±0.243	< -0.522	< -1.036	
45	17 45 22.5	-28 17 32.5	15.1	3.62 ±1.24	< -0.273	< -0.126	
46	17 45 26.1	-28 56 32.6	10.9	0.38 ±0.10 ^(M)	–	> 0.0986	CSI-28-17423 (7"; B; B=11.5;V=11.2); HD316223 (7"; G;B=1.3)
47	17 45 28.0	-29 12 4.5	26.2	1.2 ±0.3 ^(H)	< -0.462	< -1.103	IRAS 17422–2911 (51")
48	17 45 29.0	-28 09 25.1	10.3	8.37 ±1.60	< -0.866	< -0.648	
49 (12)	17 45 30.3	-29 07 06.8	2.3	9.6 ±0.499	< -0.753	0.0989 ± 0.108	
50 (8)	17 45 32.5	-28 59 47.6	25.6	<0.30	–	–	
51	17 45 32.6	-28 47 17.3	11.4	1.4 ±0.275	< -0.147	-0.0456 ± 0.371	
52 (11)	17 45 33.1	-29 05 50.0	8.0	1.0 ±0.220	< -0.2446	< -0.536	
53	17 45 39.4	-29 17 33.6	16.4	0.9 ±0.2 ^(H)	< -0.3189	< -0.642	
54 (7)	17 45 40.7	-29 00 29.4	13.7	2.46 ±0.48	< -1.145	< -1.316	SgrA* (9")
55	17 45 41.7	-29 08 52.7	17.4	0.33 ±0.10 ^(M)	–	> 0.367	
56	17 45 43.1	-28 59 36.7	18.7	5.5 ±0.5	< -1.297	< -0.684	
57 (14)	17 45 44.0	-29 13 22.9	11.2	1.6 ±0.289	< -0.427	-0.0802 ± 0.315	HD316232 (6"; O+...; B=11.1 , V=10.4)
58 (9)	17 45 44.1	-29 04 59.4	5.5	2.2 ±0.287	< -0.1869	0.0329±0.257	
59 (6)	17 45 45.6	-28 58 29.2	4.8	2.4 ±0.286	< -1.39	-0.765 ± 0.191	
60 (3)	17 45 50.7	-28 52 43.7	5.9	2.1 ±0.275	< -0.786	-0.209 ± 0.259	
61 (10)	17 45 52.5	-29 07 49.4	6.6	1.8 ±0.266	< -0.0979	-0.0926 ± 0.306	
62	17 46 01.8	-28 29 16.7	16.4	8.64 ±1.5	> 0.556	> 0.199	HD316297 (11"; K7; B=11.4; V=10.0)
63	17 46 05.5	-29 30 54.8	3.2	121 ±4.37	< -2.091	< -2.446	A1742–294 (13")
64	17 46 06.2	-29 40 9.40	13.0	3.27 ±0.80	< -0.272	< -0.0168	V734 Sgr (4"; (A1* V*?); B=13.00)
65 (5)	17 46 07.3	-28 59 50.2	5.7	1.9 ±0.271	< -0.713	< -0.558	
66	17 46 08.2	-28 17 56.4	12.5	5.12 ±1.27	–	–	
67 (2)	17 46 14.1	-28 51 44.9	18.2	4.1 ±0.623	< -1.53	< -1.26	1E 1742.9–2849 (30")
68	17 46 31.6	-28 10 29.0	13.5	3.90 ±1.15	< -0.374	< -0.713	
69 (1)	17 46 39.2	-28 53 52.4	1.8	29.5 ±0.864	< -1.00	-0.181 ± 0.060	HD316314 (0"; F0; B=9.94; V=9.51); 1E1743.4–2852 (2")
70	17 47 00.4	-29 13 1.90	8.2	18.2 ±1.42	< -1.102	-0.355 ± 0.167	
71	17 47 00.8	-30 11 27.1	25.6	8.8 ±2.54	–	–	inside the shell of the SNR G359.0–0.9
72	17 47 03.7	-29 41 2.70	17.1	3.27 ±1.05	–	> -0.0539	OH359.5–0.7(13"; Molecular Cloud); [TVH89]203(15"; Maser)

Table 3. Continued

Source ID	R.A. (J2000)	Dec. (J2000)	Error (")	cts ks ⁻¹ (0.1–2.4 keV)	Log(S/H)	Log(M/H)	Notes
73	17 47 05.3	−28 08 54.8	6.4	27.0 ±2.81	< −0.941	−0.147 ± 0.208	BN Sgr (5"); (Al* V*) F3V; B=9.60; V=9.28)
74	17 47 14.9	−30 01 57.5	17.7	3.6 ±1.2	< −0.697	< −0.378	
75	17 47 15.5	−29 58 04.3	8.0	20 ±2.48	< −1.450	< −1.62	G359.23–0.92 (The Mouse)
76	17 47 23.5	−30 00 39.3	22.4	36.2 ±3.61	< −1.189	< −1.649	
77	17 47 25.4	−30 02 40.7	3.6	126 ±6.0	< −2.046	< −2.12	SLX1744–300 (27")
78	17 47 25.9	−29 59 57.8	2.7	197.2 ±7.30	< −2.258	−1.88 ± 0.337	SLX1744–299 (15")
79	17 47 29.9	−29 58 57.7	17.3	11.0 ±2.09	< −0.567	< −1.348	
80	17 47 31.0	−28 13 46.8	5.5	31.4 ±3.64	−0.446 ± 0.353	−0.138 ± 0.258	
81	17 47 37.3	−30 10 23.9	27.6	12.6 ±3.12	< −0.8195	< −0.758	near the shell of the SNR G359.0–0.9
82	17 47 54.2	−29 59 8.4	15.3	4.1 ±1.25	–	–	
83	17 48 07.8	−29 07 58.8	13.9	4.82 ±1.13	< −0.279	< −0.673	CD-29 14004 (7"); B+...; B=11.83; V=11.05)
84	17 48 25.1	−28 44 24.5	15.7	3.19 ±0.84	< −0.200	< −0.452	
85	17 48 28.7	−29 00 33.0	12.8	3.81 ±0.96	< −0.319	< 0.00770	
86	17 48 35.3	−29 57 23.3	10.7	8.11 ±1.36	< −0.681	< −0.717	HD316341 (6"); (Em*) O+...;B=9.54;V=9.06)
87	17 48 49.4	−30 01 03.9	10.7	5.1 ±1.02	< 0.0156	< −0.420	
88	17 48 53.4	−29 08 6.70	7.5	8.19 ±1.27	< −0.363	−0.259 ± 0.353	
89	17 48 54.4	−28 59 39.2	11.0	6.55 ±1.31	< −0.0571	−0.343 ± 0.480	HD316308 (9"); K0; V=9.0)
90	17 49 25.8	−29 01 57.2	16.7	1.9 ±0.7 ^(H)	< −0.189	< −0.494	
91	17 49 28.6	−29 18 58.8	4.10	41.0 ±2.7	0.404 ± 0.169	0.0645 ± 0.191	HD161907 (6"); (*i*); B=8.33;V=8.05); CD-29 14038B (9"); (*i*);V=13.0)
92	17 49 37.8	−29 03 24.1	10.5	9.35 ±1.54	< −0.754	< −0.386	
93	17 49 41.4	−29 17 12.7	17.3	3.5 ±1.02	–	–	HD316418 (16"); F0; B=9.94; V=9.46)
94	17 50 04.9	−30 08 29.3	16.4	7.33 ±1.61	< −0.480	0.0434 ± 0.428	
95	17 50 07.3	−30 01 55.2	14.1	3.73 ±1.17	< −0.139	< −0.378	
96	17 50 24.9	−29 34 53.5	16.4	1.5 ±0.50 ^(M)	–	> 0.0794	
97	17 50 29.4	−29 00 7.2	10.3	5.93 ±1.22	< −0.717	< −1.123	1RXPJ175029.8–285957 (10")
98	17 50 33.8	−29 21 11.4	15.3	2.6 ±0.8	–	–	
99	17 50 41.3	−29 16 44.5	7.5	9.35 ±1.38	< −0.388	0.0536 ± 0.304	HD162120 (3"); (*i*) A2V; B=8.51; V=8.33)
100	17 50 58.0	−29 39 00.1	13.3	3.24 ±1.05	–	–	
101	17 51 11.1	−29 35 41.9	9.8	3.41 ±0.99	< −0.570	< −0.589	
102	17 51 25.9	−29 37 44.4	11.0	4.56 ±1.17	< −0.924	< −0.457	
103	17 51 36.7	−29 05 31.8	17.1	3.02 ±0.86	–	> 0.0793	
104	17 51 38.5	−29 50 26.3	14.8	6.69 ±1.93	< −0.563	< −0.857	
105	17 51 41.4	−29 18 49.5	12.6	4.35 ±1.28	< −0.252	< −0.356	
106	17 51 42.2	−29 45 47.4	31.0	3.5 ±1.1 ^(S)	> 0.293	–	
107	17 52 21.2	−29 04 32.2	10.9	3.9 ±1.12	< −0.608	< −0.0804	